

# 6.7 GHz methanol maser variability in Cepheus A

M. Szymczak <sup>\*</sup>, P. Wolak and A. Bartkiewicz

*Centre for Astronomy, Faculty of Physics, Astronomy and Informatics, Nicolaus Copernicus University,  
Grudziadzka 5, 87-100 Torun, Poland*

Accepted 2013 December 19. Received 2013 December 18; in original form 2013 September 6

## ABSTRACT

6.7 GHz methanol maser emission from the well-studied star-forming region Cepheus A was monitored with the Torun 32 m radio telescope. We found synchronized and anticorrelated changes of the flux density of the two blueshifted and one redshifted maser features for  $\sim 30$  per cent of 1340 d of our observations. Two of those features exhibited high amplitude flux density variations with periods of 84–87 d over the last 290 d interval of the monitoring. We also report on two flares of emission at two different redshifted velocities completely covered during the whole outburst. These flare events lasted 510–670 d and showed a very rapid linear rise and slow exponential decline, which may be caused by variability of the seed flux density. The flux density of the two strongest features dropped by a factor of 2–5 on a time-scale  $\sim 22$  yr, while other features have not changed significantly during this period, but showed strong variability on time-scales  $\lesssim 5$  yr.

**Key words:** masers – stars: formation – ISM: individual objects: Cep A – radio lines: general

## 1 INTRODUCTION

Cepheus A (Cep A) is a nearby,  $0.70 \pm 0.04$  kpc (Moscadelli et al. 2009), massive star-forming region with a bolometric luminosity of  $2.5 \times 10^4 L_{\odot}$  (Evans et al. 1981). It contains an extended ( $\sim 1$  arcmin) molecular outflow of complex morphology that is probably powered by the radio continuum source HW2 (Hughes & Wouterloot 1984). Interferometric observations of the dust continuum, free-free emission and several molecular tracers have shown that HW2 is surrounded by circumstellar discs of dust and gas of radii of  $\sim 300$  and  $\sim 600$  au, respectively (Patel et al. 2005; Curiel et al. 2006; Jimenez-Serra et al. 2007, 2009; Torrelles et al. 2011). Very long baseline interferometry (VLBI) observations of water masers revealed the presence of a slow ( $\sim 10$ – $70$  km s $^{-1}$ ) wide-angle ( $\sim 102^\circ$ ) outflow together with a high-velocity ( $\sim 500$  km s $^{-1}$ ) ionized jet with an opening angle of  $\sim 18^\circ$  associated with HW2 (Torrelles et al. 2011). 6.7 GHz methanol masers originate in an arc-like structure of size of 1350 au (Sugiyama et al. 2008a; Vlemmings et al. 2010; Torstensson et al. 2011). Torstensson et al. (2011) proposed a model in which the maser ring has a radial motion of  $1.3$  km s $^{-1}$ , probably infall, and the methanol maser emission probes the interface between the accretion flow and the disc. Polarimetric observations of the 6.7 GHz transition indicated that the magnetic field probably regulates accretion on to the disc (Vlemmings et al. 2010).

Single-dish monitoring over a period of 81 d revealed that the flux density variability of the blue- and redshifted 6.7 GHz maser features in this source is synchronized but anticorrelated (Sugiyama et al. 2008b). This finding essentially excludes a hypothesis that the

variability is caused by collisional excitation by a shock wave from a common powering source. Instead, the negative correlation can be attributed to changes in the dust temperature of the maser regions due to their distances from a common heating source and its luminosity variations (Sugiyama et al. 2008a). Galt (2003) reported a significant change in the flux density ratio of the two strongest blueshifted features over two years. The strongest feature in the spectrum, near  $-2.6$  km s $^{-1}$ , has dropped from 1410 to 815 Jy on a time-scale of 8.1 yr (Menten 1991; Szymczak, Hrynek & Kus 2000). In this paper, we report nearly 4 yr monitoring observations of Cep A at 6.7 GHz with the aim to expand our understanding of the maser variability. The results can be used to probe the environment of HW2 and could further shed light on excitation mechanisms and physical processes related to the maser emission.

## 2 OBSERVATIONS

Observations of the 6668.519 MHz methanol line were carried out using the Torun 32 m radio telescope. The target source (RA(J2000) =  $22^{\text{h}}56^{\text{m}}17^{\text{s}}.9$ , Dec.(J2000) =  $62^{\circ}01'49''.6$ ) was monitored from 2009 June to 2013 February at irregular intervals of 1–7 d with the exception of three gaps of 3–4 weeks in the monitoring campaign due to other projects of higher priority. In total, useful data were obtained at 388 epochs, in the framework of a methanol maser monitoring programme which is still going on. A dual-channel HEMT receiver was used in a frequency-switching mode. The system temperature was about 40 K on cold sky. It was measured every 5 min by injecting a signal from a noise diode of known temperature. The conversion factor of the antenna temperature to the flux density for

<sup>\*</sup> E-mail: msz@astro.uni.torun.pl

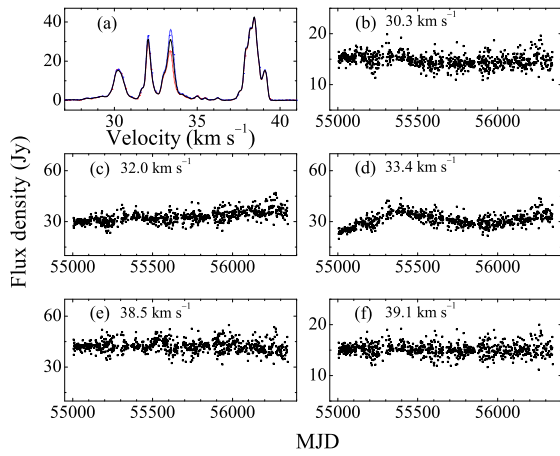


**Figure 1.** (a) Range of variation in spectrum of G32.745–0.076. The solid line is the averaged spectrum. The two dotted lines are the upper and lower envelopes. (b)–(f) Time series for strong features.

a point source was  $\sim 0.14 \text{ K Jy}^{-1}$ . The half-power beam width at 6.7 GHz was 5.5 arcmin and the rms pointing error was 22 arcsec. The two opposite circular polarizations were measured in 4 MHz bandwidth divided into 4096 channels, resulting in a velocity resolution of  $0.05 \text{ km s}^{-1}$  after Hanning smoothing. The typical rms noise level in the spectra after averaging the two polarizations was  $0.30\text{--}0.35 \text{ Jy}$ . The flux density scale was derived by continuum observations of source 3C 123, assumed to have a flux density of  $11.76 \text{ Jy}$  (Ott et al. 1994). The 32 m antenna gain reduction at low ( $15^\circ$ ) elevation angle was  $\sim 2.5$  per cent.

The maser source G32.745–0.076 previously reported as non-variable (Caswell, Vaile & Ellingsen 1995) within  $\sim 5$  per cent (Szymczak et al. 2011) was regularly observed at 801 epochs in order to check the stability of the system. Fig. 1 shows the range of variation in the spectrum of G32.745–0.076 and the time series of strong features. The emission features near  $30.3$ ,  $38.5$  and  $39.1 \text{ km s}^{-1}$  have not shown variability in excess of  $\sim 8$  per cent during the monitoring period. The other two features near  $32.0$  and  $33.4 \text{ km s}^{-1}$  show high variability of about 19 and 37 per cent, respectively. Based on the standard deviation of the flux density values of ‘non-variable’ features of this source, we estimate that our flux density calibration is better than 10 per cent.

To quantify the variability, we used the variability indices  $\nu_1$  and  $\nu_2$ . The first index is given (e.g. Aller, Aller & Hughes 1992) by

$$\nu_1 = \frac{(S_{\max} - \sigma_{\max}) - (S_{\min} + \sigma_{\min})}{(S_{\max} - \sigma_{\max}) + (S_{\min} + \sigma_{\min})} \quad (1)$$

where  $S_{\max}$  and  $S_{\min}$  are the highest and lowest measured flux densities, respectively, and  $\sigma_{\max}$  and  $\sigma_{\min}$  are the uncertainties in these measurements. This variability index is a measure of the amplitude of the variability of the source and allows for the effect of measurement uncertainties. Its value is well determined only when variability is significantly greater than measurement errors and can be negative for sources with low signal-to-noise (S/N) ratios (Aller et al. 1992).

The second variability index is defined (e.g. Edelson et al. 2002) as

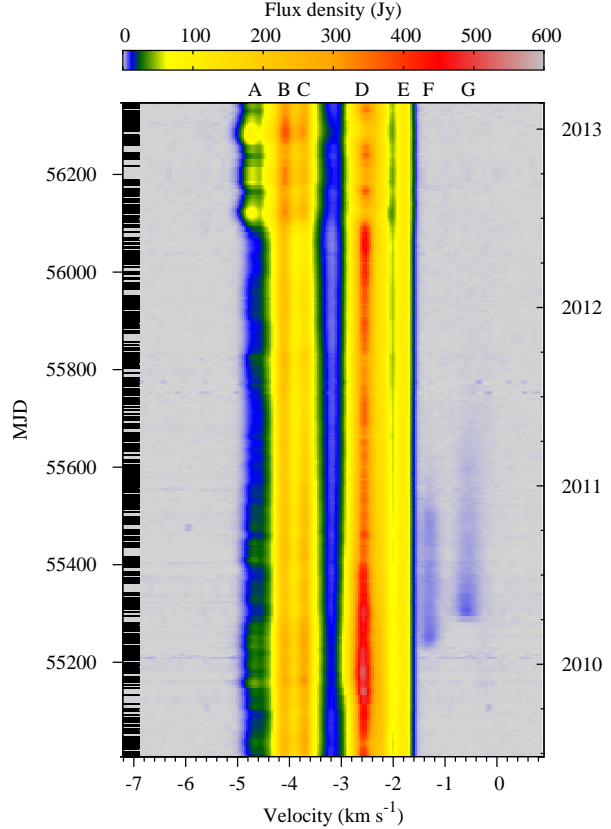


**Figure 2.** False-colour image of the 6.7 GHz methanol maser flux density over velocity and time for Cep A. The velocity scale is relative to the local standard of rest. Labels A–G indicate the analysed features. The horizontal bars in the left coordinate correspond to the dates of the observed spectra.

$$\nu_2 = \left( \frac{1}{N} \sum_{i=1}^N [(S_i - \bar{m})^2 - \sigma_i^2] \right)^{0.5} / \bar{m} \quad (2)$$

where  $N$  is the total number of observations,  $S_i$  is the observed flux density,  $\sigma_i$  is the rms level in the spectrum and  $\bar{m}$  is the average flux density. This index is a useful measure of variability for spectral channels with low S/N ratio. These variability indices are discussed in details in Aller et al. (1992) and Edelson et al. (2002).

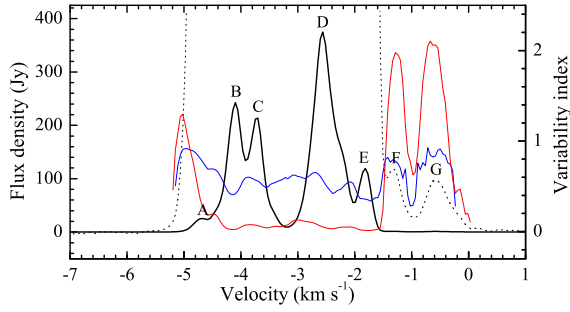
### 3 RESULTS

Changes of the 6.7 GHz methanol maser spectrum of Cep A during the monitoring campaign are shown in Fig. 2. There are five features clearly distinguished over the whole observing period and two flaring features. They are labelled as A–E and F–G, respectively (Figs 2 and 3). The average velocity of these features are listed in Table 1.

The variability index  $\nu_1$  for spectral channels with flux densities greater than  $1 \text{ Jy}$  ( $\cong 3\sigma_{\text{rms}}$ ) is plotted in Fig. 3. The two persistent features A and D and flaring features F and G have  $\nu_1$  greater than 0.61 (Table 1). Feature E has the lowest (0.36) variability index. The flaring features F and G have the highest variability index  $\nu_2$  of 1.89 and 2.03, respectively (Fig. 3, Table 1). The extreme blueshifted feature A ( $-4.66 \text{ km s}^{-1}$ ) also exhibits consider-

**Table 1.** The observed properties of the 6.7 GHz maser features.

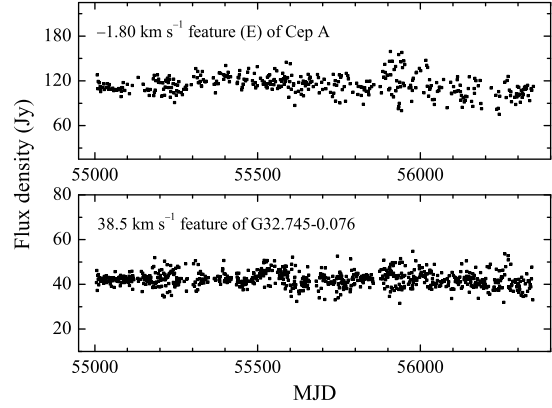
Feature	Mean velocity (km s <sup>-1</sup> )	Variability index 1 $\nu_{i1}$	Variability index 2 $\nu_{i2}$	Flux density range (Jy)	Period <sup>a</sup> (day)	Velocity drift (km s <sup>-1</sup> )	Component designation from Vlemmings et al. (2010)	Velocity range from Torstensson et al. (2011) (km s <sup>-1</sup> )
A	-4.66	0.766	0.261	7.0; 82.9	84.2±2.7	-0.10	11,12	-4.76; -4.32
B	-4.10	0.417	0.025	153; 378		<0.03	1	-4.32; -3.79
C	-3.72	0.559	0.065	90; 325		-0.06	7,8,9,10	-3.96; -3.26
D	-2.60	0.611	0.062	152; 590	87.5±7.0	+0.11	2,4,5,6	-3.44; -1.95
E	-1.80	0.359	0.013	75; 159		<0.03	3	-1.95; -1.51
F	-1.32	0.793	1.891	<0.3; 6.4		<0.03	-	
G	-0.55	0.898	2.031	<0.3; 8.5		+0.13	-	

<sup>a</sup> at significance level  $p < 0.005$  for data from MJD 56057 to 56347.**Figure 3.** Average 6.7 GHz maser line profile of Cep A (black line) with the variability indices  $\nu_{i1}$  (blue line) and  $\nu_{i2}$  (red line) superimposed. The dotted line shows the average spectrum magnified by a factor of 50 to display flaring features F and G. The mean velocities of labelled features are listed in Table 1.

able variability. Note that the variability index reaches a maximum value of 1.28 near  $-5.05$  km s<sup>-1</sup>, i.e. in the blue wing of feature A. This is due to the outburst activity of feature A which began after MJD 56083 (Fig. 2). The lowest value of  $\nu_{i2} = 0.013$  is observed in feature E.

The second variability index has the advantage that is sensitive to flaring and weakly variable features. The first index has rather a narrow range of values for the features of various levels of variability. Nevertheless, these two indices are well correlated. Feature E is one of the permanent features that show marginal variations in a 3.7 yr monitoring period. Comparison of its flux density time series with that of the strongest feature of the ‘non-variable’ source G32.745–0.076 (Fig. 4) indicates a variation of  $\sim 11.5$  per cent. This is only a few percent higher than the calibration uncertainty. This feature was previously reported as showing low ( $\sim 15$  per cent) variability on a time-scale of three months (Sugiyama et al. 2008b).

Figure 5 shows the flux density of seven features (Table 1) as a function of time. There is an indication that the changes in flux density of feature D ( $-2.60$  km s<sup>-1</sup>) are anticorrelated with the changes in flux density of features A ( $-4.66$  km s<sup>-1</sup>), B ( $-4.10$  km s<sup>-1</sup>) and C ( $-3.72$  km s<sup>-1</sup>) for MJD 55007–55115 and 56057–56347. This behaviour is clearly visible after MJD 56057 (Fig. 2), when during  $\sim 70$  d, feature D decreased in flux density by 24 per cent from its initial value, whilst features C and B increased by 233 and 165 per cent, respectively. Feature A experienced an increase by a factor

**Figure 4.** Time series of feature E ( $-1.80$  km s<sup>-1</sup>) of Cep A and the strongest feature of G32.745–0.076.

of 8.4 (Fig. 5). Changes in flux density reversed after MJD 56127 when during  $\sim 37$  d feature D increased by 86 per cent while feature A dropped to 250 per cent of the values observed on MJD 56057. No obvious decline in flux density was seen for features B and C between MJD 56127 and 56164. The synchronized variations of features A and D continued until the end of the monitoring period. The flux density of feature D varied inversely to that of features B and C from MJD 56290 to 56347.

Fig. 6 shows correlation plots for feature D versus features A and B. The correlation coefficients were  $-0.82$  and  $-0.59$ , respectively for the data from MJD ranges 55007–55115 and 56057–56347. A positive correlation was seen over a 2.5 yr period from MJD 55133 to 56052. Correlation coefficients for the variation of all the persistent features during the time spans are listed in Table 2. We conclude that the synchronized and anticorrelated variations occurred for pairs of features A and D, and B and D, i.e. between the blue- and redshifted emission, for intervals of 110 and 290 d, which in total is about 30 per cent of our monitoring period. Sugiyama et al. (2008b) observed similar variations over a 80 d monitoring period.

After MJD 56057 the emission showed apparent periodic changes (Fig. 5). The Lomb–Scargle periodogram (Scargle 1982) shows statistically significant periods of 84.2 and 87.5 d for features A and D, respectively (Table 1). No statistically significant periodicities are found for the other features.

The peak velocities of the main features were measured by

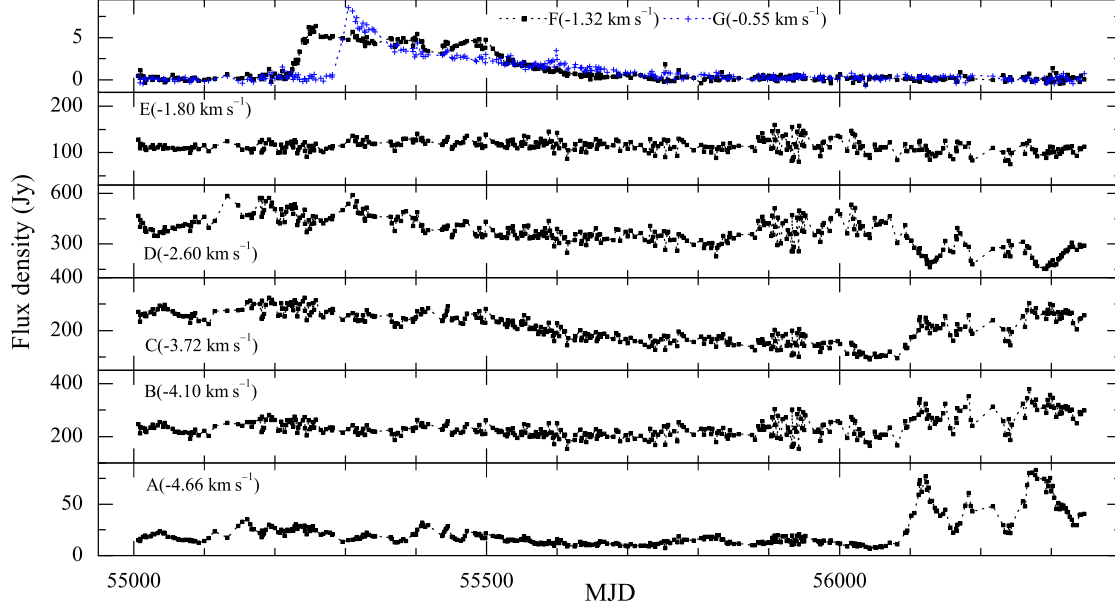


**Figure 5.** Time series of the flux density of selected features.

**Table 2.** Correlation coefficients for different time spans. Significant ( $p < 0.0001$ ) correlations are shown in bold.

Feature	MJD 55007–55115 & 56057–56347				Feature	MJD 55133–56052			
	A	B	C	D		A	B	C	D
B	<b>0.87</b>					<b>0.65</b>			
C	0.33	<b>0.47</b>				<b>0.85</b>	<b>0.55</b>		
D	<b>-0.82</b>	<b>-0.59</b>	-0.07			<b>0.55</b>	<b>0.74</b>	<b>0.63</b>	
E	-0.06	0.31	0.38	<b>0.56</b>		0.19	<b>0.77</b>	0.26	<b>0.54</b>

parabolic fitting to the three brightest channels. The values of velocity drifts are listed in Table 1. The peak velocity of feature A shows a sudden decrease of  $0.10 \text{ km s}^{-1}$  after MJD 56092 (Fig. 7) with increasing flux density (Fig. 5) and the velocity increased with decreasing flux density. The amplitude of velocity changes during three consecutive bursts was  $0.08 \text{ km s}^{-1}$  and the velocity of the peak during the flux minima decreased by  $0.04 \text{ km s}^{-1}$  over a period of 240 d. These velocity shifts could be caused by variability in one of a pair of spectrally blended features with almost the same but slightly different velocities. It is possible that the lower velocity feature is more stable whilst the higher velocity feature experiences strong variability (e.g. Peng 1989). This is plausible explanation because MERLIN data imply that feature A is composed of two components with velocities which differ by  $0.11 \text{ km s}^{-1}$  (Vlemmings et al. 2010). Moreover, at some epochs, this emission was not easily detected in VLBI observations (Torstenson et al. 2011). Similar amplitude variations were seen for feature C but with no significant velocity change exceeding  $0.05 \text{ km s}^{-1}$ . Feature D showed an increase of up to  $0.11 \text{ km s}^{-1}$  in the peak velocity, with peri-

odic modulations after MJD 56092 (Fig. 5), wherein the velocity increased with decreasing flux density. As flaring feature G was relatively weak and well separated from the rest of the features (Fig. 5), Gaussian fitting was used to measure the peak velocity. There was a  $0.13 \text{ km s}^{-1}$  increase of peak velocity over a time span of 490 d when its flux density decreased from 8.7 to  $\sim 0.9 \text{ Jy}$  ( $3\sigma$  limit). Note that the decline of feature G is correlated with a lowering of flux density in the rest of the features (Fig. 5). We conclude that three persistent features showed velocity drifts by 2–3 spectral channels. The periodic flux density variations which are linked to these small velocity drifts argue against their origin in any systematic radial outflow or infall; they are more likely to be due to flux density variations in blended components.

Multi-Element Radio-Linked Interferometer (MERLIN) data (Vlemmings et al. 2010) suggest that the emission by features identified in the single-dish spectrum comes from spatially separated components (Fig. 8). Our features A, C and D consist of up to four components (Table 1) distributed in clumps elongated by 180–570 mas, which corresponds to projected linear sizes of

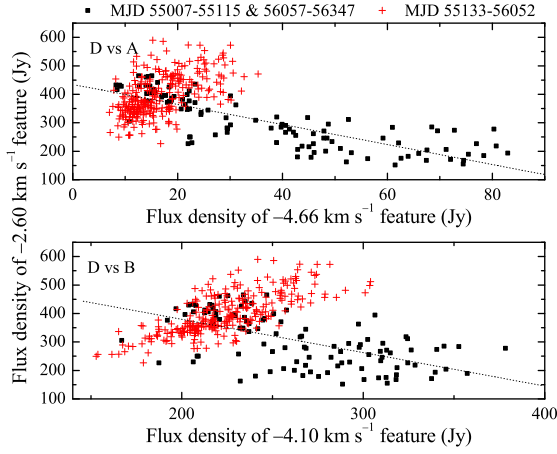


**Figure 6.** Comparison of flux densities of the strongest redshifted feature D with those of blueshifted features A and B. Symbols in both panels refer to the time spans given in the legend. The dotted lines show the best fits to the data marked by squares.

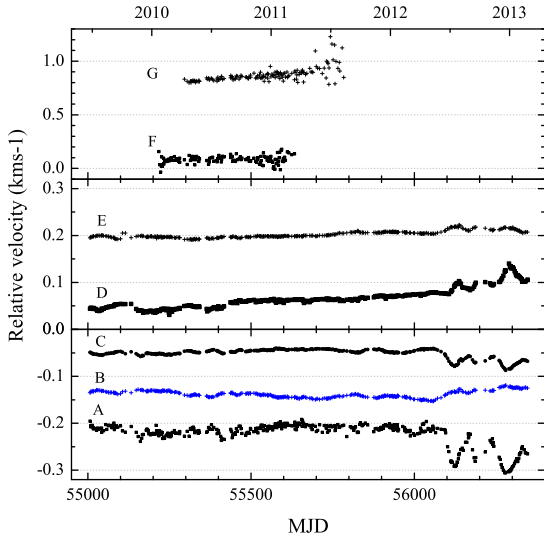


**Figure 7.** Time series of the relative velocities of peak emission of the main features. The labels of features are given in Table 1.

130–400 au at a distance of 700 pc (Moscadelli et al. 2009). VLBI observations (Torstensson et al. 2011, their fig. 2 and table 3) suggest that our feature C is a blend of three components in the velocity range from  $-3.96$  to  $-3.26$  km s $^{-1}$ , whereas feature D is a blend of more than three components. The velocity ranges of our individual features as deduced from the VLBI data are listed in Table 1. We conclude that our observations of features C and D probe the variability of multiple spatially different parts of the ring-like distribution of  $\sim 650$  au radius. Their indices of variability are of intermediate values. Feature A, which has the highest variability, appeared as a blend of two components in the MERLIN observation in 2006 December (Vlemmings et al. 2010) and in the VLBI

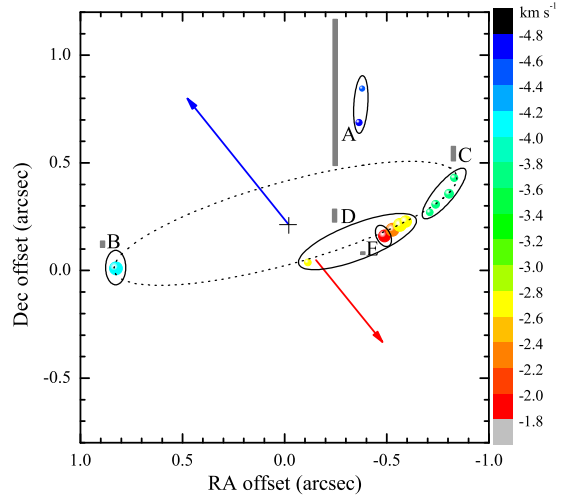


**Figure 8.** 6.7 GHz maser components in Cep A (Vlemmings et al. 2010) with variability index information. The groups of maser components marked with ellipses and letters correspond to the features identified in the single-dish spectra (Table 1). The length of the vertical bars is proportional to the variability index  $v_{i2}$ . The size and colour of symbols correspond to the logarithm of brightness and velocity, respectively. The dotted ellipse shows the best fit to the maser distribution with the central 7 mm continuum object (Curiel et al. 2006) marked by the cross symbol. The arrows mark the blue- and redshifted lobes of the collimated radio outflow (Curiel et al. 2006).

data from 2004 November (Torstensson et al. 2011). It seems that this emission does not belong to the arc-like distribution. Feature B, showing moderate variability, appears to correspond to the eastern component with a Gaussian profile (Torstensson et al. 2011, their fig. 2). The VLBI data suggest that emission from feature E, which has the lowest variability indices, comes from a component with a Gaussian profile that is displaced by only  $\sim 50$  mas from the strongest component of feature D. We conclude that our single-dish data provide reliable information for the variability of maser components isolated in velocity and unresolved with by the MERLIN beam-size of  $40 \times 30$  mas.

### 3.1 Flares

Two new emission features F ( $-1.32$  km s $^{-1}$ ) and G ( $-0.55$  km s $^{-1}$ ) appeared in the source (Table 1, Fig. 5). The light curves are rather complex and we obtained the best fits to their rising parts using linear function and to their declining parts using exponential functions ( $S_{\nu} \propto e^{-t/\tau_d}$ ). The epochs of the start and the peak of each flare are given in Table 3. The times taken to rise from the  $1\sigma_{\text{rms}}$  level of  $\sim 0.3$  Jy to their peak flux densities,  $t_r$ , were 37 and 24 d, for features F and G, respectively. Note that the rising part of the light curve of feature F was well sampled but for that of feature G the observations were sparse. Therefore, the rise time of feature G is less certain than that of feature F. Declining parts of the two light curves were fitted by two different exponential laws for two intervals  $\Delta t_1$  and  $\Delta t_2$  (Table 3). The corresponding decay time-scales  $\tau_{d1}$  and  $\tau_{d2}$  for feature F were 158 and 67 d while for feature G they were 37 and 251 d, respectively. The flares of emission of features F and G were seen over 513 and 670 d, respectively, and the corresponding



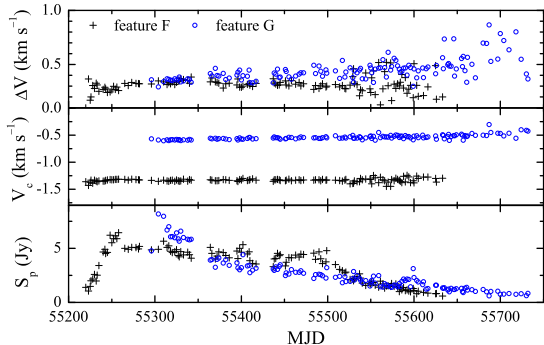


**Figure 9.** Time series of the peak flux density ( $S_p$ ), the velocity of the peak ( $V_c$ ) and the line-width at half-maximum ( $\Delta V$ ) of the flaring features F and G.

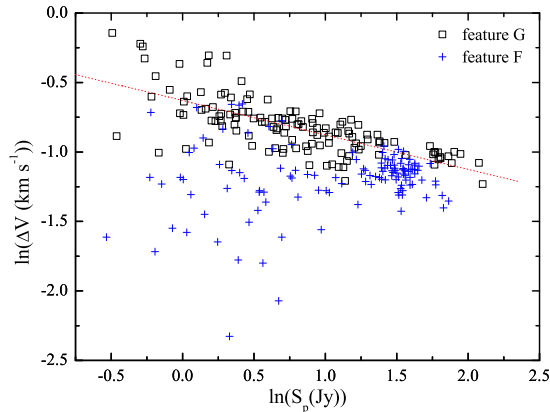


**Figure 10.** Relationship between the line-width ( $\Delta V$ ) and the flux density ( $S_p$ ) for the flaring features. The dotted line marks the best fit for the feature G.

ratios of the rise time to the decay time,  $R_{rd}$ , were 0.08 and 0.04. The time delay between these flares was  $\sim 60$  d.

The rapid rises in the flares were not associated with a rapid rise in the total methanol maser luminosity of the source. Flares with similar characteristics such as this have not previously been observed to our knowledge in any methanol source (Goedhart, Gaylard & van der Walt 2004; Fujisawa et al. 2012). A strong OH 1665 MHz maser flare with a rise time of  $\sim 16$  months was reported from Cep A (Cohen & Brebner 1985). Several rapid bursts were also observed in its 22 GHz water maser line with typical rise and decay times of 3–30 d (Mattila et al. 1985). No MERLIN or VLBI observations are available which show the location of the flaring maser components F and G.

The profiles of the flaring features are well separated in velocity and not blended. We fitted Gaussian curves to the observed line profiles of features F and G, obtaining the peak flux density,  $S_p$ , and the velocity of the peak,  $V_p$  and the full width at half-maximum of the line-width,  $\Delta V$ . Fig. 9 shows the variations of these three parameters. Feature F did not show significant variations in  $V_p$  and  $\Delta V$ . Note that with decreasing peak flux density the accuracy of fit-

ting drops such that the scatter in  $\Delta V$  gradually increases and individual estimates of less than  $0.2 \text{ km s}^{-1}$  and higher than  $0.45 \text{ km s}^{-1}$  are less reliable.

Feature G exhibited a systematic shift in radial velocity of  $0.12 \text{ km s}^{-1}$  and an increase in line-width from  $0.33$  to  $0.56 \text{ km s}^{-1}$ , as the flux density decreased over a time span of 436 d during which the parameters could be measured with sufficient accuracy. Fig. 10 shows the dependence of the line-width on the flux density. The least-squares fit to the data of feature G gives the relationship  $\ln \Delta V / \ln S_p = -0.25 \pm 0.02$ . This can be interpreted as a result of line narrowing during maser amplification. The narrowing is a shallower function of intensity than that which is predicted by the standard theory of unsaturated masers, i.e.  $\ln \Delta V / \ln S_p = -0.5$  (Goldreich & Kwan 1974; Mattila et al. 1985). The weak dependence of the line-width on the flux density for feature G and the constant line-width for feature E is poorly consistent with this theory. One can suggest that either the flares are behaving differently from the persistent components and are at least partially saturated, and/or the flares are line-broadened by some other mechanism such as turbulence (Vlemmings et al. 2010).

## 4 DISCUSSION

Our densely sampled observations of Cep A over the past 3.7 yr allow us to study its 6.7 GHz maser emission behaviour and obtain two main results.

(i) Synchronized and anticorrelated flux density variations, of moderate or large amplitude, were seen from the blueshifted features A and B and the redshifted maser feature D, on time-scales of 110 and 290 d. Periodic variability (84–87 d) of features A and D was identified during the last 290 d of the monitoring period.

(ii) Two flares, with durations of  $\sim 510$  and  $\sim 670$  d, appeared at two different velocities in the redshifted part of the spectrum. The time delay between the flares was  $\sim 60$  d. None of the persistent features A–E in the maser spectrum showed any signs of variability similar to the very rapid rise and a slow decay exhibited by features E and G.

The synchronized and anticorrelated variability of methanol maser features at the blue- and redshifted velocities in Cep A was first discovered by Sugiyama et al. (2008b) during a monitoring period of 81 d. Our observations indicate that this phenomenon of varying intensity occurred for the two pairs of features for a total of  $\sim 400$  d at the beginning and the end of our monitoring period. High angular resolution maps of 6.7 GHz methanol masers (Sugiyama et al. 2008b; Vlemmings et al. 2010; Torstensson et al. 2011) suggest that variability is synchronized between different parts of an arched structure. In particular, when the flux density of the blueshifted maser components to the east and north (features B and A in Fig. 8) increases, the flux density of the redshifted component to the south-west (feature D in Fig. 8) decreases, and vice versa.

The maps of dust continuum, radio continuum and lines (Curiel et al. 2006; Torrelles et al. 2011, their fig. 5) imply that in projection the redshifted emission is closer to the main heating source (Jimenez-Serra et al. 2009) than the blueshifted emission. As the methanol maser is probably excited by infrared radiation from warm dust (Cragg, Sobolev & Godfrey 2005), the observed variability can be attributed to changes in dust temperature due to luminosity variations in the heating source (Sugiyama et al. 2008b). They argued that if the luminosity increases, the dust temperature near the source would be too high to sustain the maser emission, whilst still being cool enough (100–200 K) to allow masing fur-

**Table 3.** Parameters of the flaring features.

Feature	Epoch of start (MJD)	Epoch of peak (MJD)	Amplitude (Jy)	$t_r$ (d)	$\Delta t_1$ (MJD)	$\tau_{d1}$ (d)	$\Delta t_2$ (MJD)	$\tau_{d2}$ (d)
F	55217 $\pm$ 3	55254 $\pm$ 3	6.3	37 $\pm$ 3	55254–55503 $\pm$ 3	158 $\pm$ 50	55503–55730 $\pm$ 8	67 $\pm$ 4
G	55281 $\pm$ 5	55305 $\pm$ 5	8.5	24 $\pm$ 7	55305–55378 $\pm$ 4	37 $\pm$ 11	55378–55950 $\pm$ 10	251 $\pm$ 15

ther from the source. In turn, decreasing luminosity in the heating source would allow masers closer to the source but be too cold further away. This interpretation is poorly consistent with the ring model (Vlemmings et al. 2010; Torstensson et al. 2011) where almost all clouds are located at  $\sim 650$  au from the central object. It appears that at least features A and D (Fig. 8) lie at similar distances from the 7 mm source which is probably the central exciting object. Changes in dust temperature due to variability in this object are thus unlikely to cause the anticorrelated changes in the flux densities of these maser features.

Jimenez-Serra et al. (2007) describe results which suggest a molecular disc around HW2 with a velocity gradient of  $\sim 5$  km s $^{-1}$ . If this is in Keplerian rotation, an observer in a given direction close to the plane of the disc will see the brightest masers along lines through the centre of rotation and through the tangential limbs of the disc (Elmegreen & Morris 1979, their fig. 1), giving rise to a characteristic triple-peaked profile (Cesaroni 1990). This can be explained first by considering isotropic masing in the reference frame of the disc; segments separated by  $180^\circ$  have similar radial velocities with respect to the centre and thus maser emission from one side of the disc can be amplified further by material on the opposite side. Secondly, from the point of view of a distant observer located in a plane close to the disc plane, the smallest velocity gradients, and hence, the strongest maser amplification in the direction of the observer, are located towards the centre and the tangents of the disc. In this model, the diametrically opposite sections of disc are in radiative contact with the other. Cesaroni (1990) have shown that if the pump rate drops on one side of the disc then the opposite side will be affected soon after a time equal to the light crossing time. As a result the blueshifted emission will be anticorrelated with the redshifted emission or vice versa. However, this interpretation is not fully satisfactory because although the VLBI data suggest a ring model, the dominant maser motion is radial, at  $1.3$  km s $^{-1}$ , not Keplerian rotation (Torstensson et al. 2011). The observed velocities of the maser components suggest infall towards the central object (Vlemmings et al. 2010; Torstensson et al. 2011). It may be possible to derive a model for the synchronized variations of maser features in Cep A, including the effects of changes in one part of the ring on emission in other parts, if the 3D velocity field can be determined from proper motion measurements.

#### 4.1 Flaring features

Flare events in the 6.7 GHz maser line are very scarce. Goedhart et al. (2004) monitored 54 maser sources for 4 yr and found a flaring feature only in one source, i.e. G351.42+0.64. The variability pattern of the  $-5.88$  km s $^{-1}$  feature in this source is similar to that of features F and G of Cep A; its duration was  $\sim 340$  d,  $R_{rd} \approx 0.1$ , it fell exponentially for two time intervals. This flare had a maximum flux density of about 230 Jy, much stronger than the flare maxima of 6.3 and 8.5 Jy in Cep A. Quasi-periodic flare phenomena of similar patterns but with much shorter decay time-scales of 5–30 d and  $R_{rd}$  of 0.17–0.20 were reported in methanol masers

G33.64–0.21 and G37.55+0.20 (Araya et al. 2010; Fujisawa et al. 2012). Other methanol sources with periodic behaviour are known, such as G22.357+0.066 with  $R_{rd} = 0.34$  (Szymczak et al. 2011) and G9.62+0.20E with  $R_{rd} = 0.37$  (Goedhart, Gaylard & van der Walt 2003). Note that, in periodic and quasi-periodic sources, flaring activity usually shows correlated variations across several different features in the spectrum, but the behaviour of flaring features in Cep A and G351.42+0.64 was completely unrelated to the other features. This indicates that these changes are restricted to a local volume of the gas.

The emission at velocities of  $-0.53$  to  $-0.36$  km s $^{-1}$ , which may correspond to feature G, was detected on MJD 53987 in the VLBI observation but not in the single-dish study (Sugiyama et al. 2008b). It appears to coincide with the southern part of the radio continuum jet of HW2 and with the cluster of maser clumps with velocities of  $-3$  to  $-2$  km s $^{-1}$  (Sugiyama et al. 2008b) also seen in the maps taken with the EVN on MJD 53315 (Torstensson et al. 2011, their fig. 1) and with MERLIN on MJD 54072 (Vlemmings et al. 2010). No emission near  $-0.5$  km s $^{-1}$  was detected at these two epochs. This suggests that feature G undergoes variations of much higher amplitude than those measured with the 32 m dish. Adopting a quiescent value of 0.035 Jy (the sensitivity limit of the EVN observations; Torstensson et al. 2011) the flux density of the feature has risen by a factor of up to 240. The diameter of the cluster is  $\sim 40$  au (Torstensson et al. 2011) for the source distance of 700 pc (Moscadelli et al. 2009) and the velocity dispersion of the maser clumps is up to  $2.5$  km s $^{-1}$ . Torstensson et al. (2011) argued that the velocity field of the methanol masers in Cep A indicates a modest infall of maser clumps. The ring structure is probably the interface between the accretion flow and disc. Direct measurements of infall of methanol maser clouds towards a high-mass young star were reported by Goddi, Moscadelli & Sanna (2011).

The above discussion may suggest that flaring features F and G arise in a small region lying in front of the continuum emission of the radio jet from HW2. The flux density and morphology of this radio continuum is time variable (Curiel et al. 2006). In such circumstances, maser emission from these features can easily be affected by several factors such as changes in path length, pump rate and background emission (Caswell et al. 1995; Cragg et al. 2005; van der Walt, Goedhart & Gaylard 2009).

Fujisawa et al. (2012) proposed a fast ( $\sim 1$  d) injection of energy, released for instance due to magnetic field reconnection, into a small region, as a plausible mechanism behind the maser flare in source G33.64–0.21. This energy heats the gas and dust, increasing the infrared flux density which is the main pumping agent of the 6.7 GHz transition (Cragg et al. 2005). Typical magnetic reconnection events are, however, too short to explain the 24–37 d rise times of features F and G. The dust cooling time is only 1.2 d even in the optically thick case (van der Walt et al. 2009), which is about two orders of magnitude shorter than the decay times of the flares we have observed. Thus, this model cannot be applied to our source.

It is postulated that the velocity field of the 6.7 GHz masers in Cep A signifies infall motion (Vlemmings et al. 2010; Torstensson

et al. 2011). For a flow velocity of  $1.3 \text{ km s}^{-1}$  (Torstensson et al. 2011), a maser cloud with a characteristic size of 3 au and brightness temperature of  $3 \times 10^{12} \text{ K}$  (Menten et al. 1992) could move only 0.4–0.5 au in 510–670 d. This suggests negligible changes in the cloud environment.

van der Walt et al. (2009) proposed that the declining part of methanol maser flares in periodic source G9.62+0.20E can be ascribed to a change in the background photon flux density from a recombining thermal plasma. They found characteristic decay times from 40 to 400 d for electron densities from  $10^6$  to  $10^5 \text{ cm}^{-3}$ . This range of  $\tau_d$  is fully consistent with the observed values for features F and G (Table 3). The model of van der Walt (2011) reproduces well the exponential decay of flux density we have observed.

The location of the flaring maser features is not certain but, as mentioned above, it has been suggested that they lie in the front of radio lobes with an electron density of about  $3\text{--}5 \times 10^4 \text{ cm}^{-3}$  and recombination times of 800–1300 d (Curiel et al. 2006) for a recombination coefficient of  $2.95 \times 10^{-13} \text{ cm}^3 \text{ s}^{-1}$ . The radio lobes of HW2 have persisted for a long time but episodes of ejection separated by 1.85 yr were observed (Curiel et al. 2006). We conclude that the observed characteristics of flaring features F and G can be explained by variability in the seed photon flux density. This scenario could be verified by simultaneous VLBI observations of the maser line and radio continuum, at epochs guided by single-dish monitoring.

## 4.2 Long-term variability

The spectra available in the literature (Menten 1991; Sugiyama et al. 2008a,b; Vlemmings 2008), in the Torun 32 m telescope archive and seven evenly sampled spectra from the data set reported in this paper (Figs 2 and 5) have been compiled to obtain a long-term light curve. The discovery spectrum (Menten 1991) was corrected for the rest frequency of 6668.5192 MHz (Muller, Menten & Mader 2004). The other archival spectra have been used as they were published since differences in rest frequencies have a negligible impact on the velocity scale. The light curves of the main features are shown in Fig. 11. Feature D declined by a factor of 5.2 over a period of 21.6 yr. Its light curve is best fitted by an exponential function with a decay time-scale of  $7.39 \pm 1.39$  yr. The feature was clearly non-Gaussian during the discovery observation (Menten 1991) and a shoulder at  $-2.3 \text{ km s}^{-1}$ , corresponding to a second feature, appeared on MJD 51674. Feature B shows a significant linear decay of  $8.7 \pm 2.0 \text{ Jy yr}^{-1}$ . A tentative linear decay of  $3.1 \pm 1.5 \text{ Jy yr}^{-1}$  is observed for feature A. Note that for this feature the ratio between the maximum and the mean flux density is 2.80. The peak flux densities of features C and E are fairly steady over 21.6 yr. The emission near  $-0.7 \text{ km s}^{-1}$ , with a peak flux ranging from 3.2 to 6.8 Jy, was seen during the MJD range of 51536–51844. The data imply that the declining part of a flare event was detected. At those epochs, the precision of radial velocity measurements was  $\pm 0.5 \text{ km s}^{-1}$ , which makes impossible to infer whether its peak velocity coincides with that of the recently detected feature G.

We conclude that the two strongest features, B and D, dropped in flux density by factors of 1.7 and 5.2 respectively, on a time-scale of  $\sim 22$  yr. The other features do not show significant changes on this long-term time-scale but they display significant variability on time-scales of less than 5 yr. The VLBI map (Torstensson et al. 2011) suggests that the emission of feature D comes from the same cluster of clouds (clumps *c*, *d*, *e* in their figs 1 and 2) where from the emission of stable feature E (clump *c*, therein) arises. The kinematic model of the maser structure in Cep A with a radial velocity

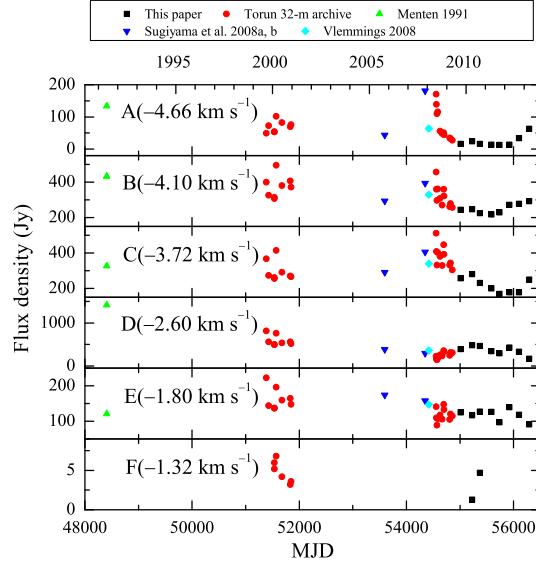


**Figure 11.** Long-term,  $\sim 22$  yr, light curves of main maser features labelled as in Fig. 3. The data before 2009 are taken from Menten (1991), Sugiyama et al. (2008a,b), Vlemmings (2008) and the Torun 32 m telescope archive. For clarity only some of the data presented in this paper (Figs 2 and 5) are repeated here. Errors in absolute flux density calibration are within 12–20 per cent.

of  $1.3 \text{ km s}^{-1}$ , proposed by Torstensson et al. (2011), implies that the displacement of maser clouds would be only  $\sim 6$  au after 21.6 yr. This can be ruled out as the cause of selective decline of the maser intensity from some clouds in the same cluster.

Ellingsen (2007) analysed the 6.7 GHz methanol maser spectra of 21 sources and estimated the percentage of spectral features that either appear or disappear over a 10 yr period. He deduced that the average lifetime of an individual methanol maser feature is approximately 150 yr. Our comparison of the present and archival data imply that feature D showing an exponential decay and features B and C with linear decays will disappear after  $\sim 50$  yr since the discovery. The other persistent features in Cep A have probably longer lifetime.

## 5 CONCLUSIONS

We have studied the 6.7 GHz methanol maser variability of Cep A based on 388 d of monitoring spaced over about 1340 d. We have found synchronized and anticorrelated flux density variations in two blueshifted features A and B, and one redshifted feature D over two periods of a total duration of  $\sim 400$  d. This behaviour well constrains causes of variability, excluding shocks from an exciting source and supporting the disc model, where the maser amplification is switched between radial and tangential modes. Although the methanol masers are probably not in a Keplerian disc (Torstensson et al. 2011), they are located in a ring showing either outfall or inflow, and changes in excitation conditions could lead to maser amplification switching between radial and tangential modes. Two flares of emission at redshifted velocities (features F and G) lasted 510–670 d. Another flare at a similar velocity was identified in the archival data. The light curves of the flares show a rapid rise followed by a slow exponential decline. The tentative location of the



flaring clouds at the front of the radio jet from HW2 may suggest that the flares are the results of variability in the seed flux density.

These explanation could be tested by simultaneous high resolution observations of the maser and radio continuum emission guided by single-dish monitoring.

## ACKNOWLEDGEMENTS

We would like to thank the referee Simon Ellingsen for constructive comments that improved the manuscript. We would also like to thank Anita Richards and Johan van der Walt for their valuable comments and Karl Menten and Wouter Vlemmings for kindly sharing their archival spectra in digital form with us. The work was supported by the Polish National Science Centre grant 2011/03/B/ST9/00627.

## REFERENCES

- Aller M.F., Aller H.D., Hughes P.A., 1992, *ApJ*, 399, 16
- Araya E.D., Hofner, P., Goss, W.M., Kurtz S., Richards A.M.S., Linz H., Olmi L., Sewilo M., 2010, *ApJ*, 717, L133
- Caswell J.L., Vaile R.A., Ellingsen S.P., 1995, *PASA*, 12, 37
- Cesaroni R., 1990, *A&A*, 233, 513
- Cohen R.J., Brebner G.C., 1985, *MNRAS*, 216, 55
- Cragg D.M., Sobolev A.M., Godfrey P.D., 2005, *MNRAS*, 360, 533
- Curiel S. et al., 2006, *ApJ*, 638, 878
- Edelson R., Turner T.J., Pounds K., Vaughan S., Markowitz A., Marshall H., Dobbie P., Warwick R., 2002, *ApJ*, 568, 610
- Ellingsen S.P., 2007, *MNRAS*, 377, 571
- Elmegreen B.G., Morris M., 1979, *ApJ*, 229, 593
- Evans N.J. et al., 1981, *ApJ*, 244, 115
- Fujisawa K. et al., 2012, *PASJ*, 64, 17
- Galt J., 2003, *AJ*, 126, 1967
- Goddi C., Moscadelli L., Sanna A., 2011, *A&A*, 535, L8
- Goedhart S., Gaylard M.J., van der Walt D.J., 2003, *MNRAS*, 339, L33
- Goedhart S., Gaylard M.J., van der Walt D.J., 2004, *MNRAS*, 355, 553
- Goldreich P., Kwan J., 1974, *ApJ*, 190, 27
- Hughes V.A., Wouterloot J.G.A., 1984, *ApJ*, 276, 204
- Jimenez-Serra I., Martin-Pintado J., Rodriguez-Franco A., Chandler C., Comito C., Schilke P., 2007, *ApJ*, 661, L187
- Jimenez-Serra I., Martin-Pintado J., Caselli P., Martin S., Rodriguez-Franco A., Chandler C., Winters J.M., 2009, *ApJ*, 703, 157
- Mattila K., Holsti N., Toriseva M., Anttila R., Malkamaki L., 1985, *A&A*, 145, 192
- Menten K.M., 1991, *ApJ*, 380, L75
- Menten K.M., Reid M.J., Pratap P., Moran J.M., Wilson T.L., 1992, *ApJ*, 401, L39
- Moscadelli L., Reid M.J., Menten K.M., Brunthaler A., Zheng X.W., Xu Y., 2009, *ApJ*, 693, 406
- Muller H.S.P., Menten K.M., Mader H., 2004, *A&A*, 428, 1019
- Ott M., Witzel, A., Quirrenbach A., Krichbaum T.P., Standke K.J., Schalinski C.J., Hummel C.A., 1994, *A&AS*, 284, 331
- Patel N.A. et al., 2005, *Nature*, 437, 109
- Peng R.S., 1989, *A&A*, 216, 173
- Scargle J.D., 1982, *ApJ*, 263, 835
- Sugiyama K., Fujisawa K., Doi A., Honma M., Kobayashi H., Bushimata T., Mochizuki N., Murata Y., 2008b, *PASJ*, 60, 23
- Sugiyama K., Fujisawa K., Doi A., Honma M., Isono Y., Kobayashi H., Mochizuki N., Murata Y., 2008a, *PASJ*, 60, 1001
- Szymczak M., Hrynek G., Kus A.J., 2000, *A&AS*, 143, 269
- Szymczak M., Wolak P., Bartkiewicz A., van Langevelde H.J., 2011, *A&A*, 531, L3
- Torrelles J.M. et al., 2011, *MNRAS*, 410, 627
- Torstensson K.J.E., van Langevelde H.J., Vlemmings W.H.T., Bourke S., 2011, *A&A*, 526, A38
- van der Walt D.J., 2011, *AJ*, 141, 152
- van der Walt D.J., Goedhart S., Gaylard M. J., 2009, *MNRAS*, 398, 961
- Vlemmings W.H.T., 2008, *A&A*, 484, 773
- Vlemmings W.H.T., Surcis G., Torstensson K.J.E., van Langevelde H.J., 2010, *MNRAS*, 404, 134